Steel and Composite Structures, *Vol. 56, No. 5 (2025) 375-382*
https://doi.org/10.12989/scs.2025.56.5.375

Failure behavior of earth dam simulated using material point method: Effect of strength parameters

Juik Son[1a], Dong-Ju Kim[2b], Hyungjoon Seo[3c] and Yong-Hoon Byun[*1]

[1]*Department of Agricultural Civil Engineering, Kyungpook National University, 80 Daehak-ro, Buk-gu, Daegu 41566, Republic of Korea*
[2]*School of Civil, Environmental and Architectural Engineering, Korea University, 145, Anam-ro, Seongbuk-gu, Seoul 02841, Republic of Korea*
[3]*Department of Civil Engineering, Seoul National University of Science and Technology, 232 Gongneung-ro, Nowon-gu, Seoul 01811, Republic of Korea*

(Received May 25, 2025, Revised July 16, 2025, Accepted July 19, 2025)

Abstract. This study investigates the failure behavior of earth dams in response to various shear strength parameters using a two-phase material point method (MPM). A total of 20 numerical dam models are developed by systematically varying the cohesion and internal friction angle of the embankment fill material. The failure evolution and displacement distributions of these models are analyzed using the two-phase MPM, while the factor of safety (FS) is determined using the finite element method. Based on the numerical results, lower cohesion and friction angles lead to more pronounced displacements and lower FS values. For sand-filled dam models, the displacement and FS are both highly sensitive to changes in the strength parameters. Conversely, clay-filled dam models exhibit minimal displacement despite displaying significant reductions in FS to values near unity. Therefore, the response of earth dams to strength parameters depends strongly on the soil type, and interpreting the displacement and FS together can facilitate reliable stability evaluation.

Keywords: earth dam; material point method; factor of safety; large-deformation analysis; shear strength parameters

1. Introduction

Earth dams are commonly used for water storage, flood control, and irrigation. However, the failure of an earth dam can have devastating consequences, including severe flooding, loss of life, extensive property damage, and significant economic disruption. Therefore, the stability of earth dams must be accurately assessed to mitigate such risks. Many researchers have focused on identifying the failure mechanisms of earth dams through field surveys, scaled model tests, and numerical simulations (Beek *et al*. 2010, Salmasi *et al*. 2020, Kim *et al*. 2023, Rajabian 2023, Al-janabi *et al*. 2024, Kim *et al*. 2024a).

The finite element method (FEM), often combined with the limit equilibrium method, is widely used to estimate the factor of safety (FS) of earth dams. The strength reduction method, which involves progressively reducing shear strength parameters until the model fails to converge, can also be combined with the FEM for a more refined analysis. However, while the FEM is adequate for small-deformation problems, it struggles to accurately capture post-failure behavior, due to mesh distortion. The discrete element method is effective for modeling large deformations in soils as it enables simulations of grain–fluid interactions (Kumar *et al*. 2012, Capecelartro and Desjardins 2013, Kodicherla 2023). Smoothed particle hydrodynamics, a meshless method, discretizes the analysis domain into particles with smoothed material properties (Bui *et al*. 2008). Despite their advantages, however, the aforementioned methods exhibit several limitations, such as difficulties in the application of boundary conditions and modeling particle contact (Soga *et al*. 2016, Qin *et al*. 2022).

The material point method (MPM) has emerged as a promising alternative for modeling large deformations in history-dependent materials (Sulsky *et al*. 1994). In the MPM, a body is represented by a set of material points carrying information related to parameters such as mass, velocity, stress, and strain. The material points move through a fixed computational grid, which is used to solve the governing equations. By combining Lagrangian particles with an Eulerian background mesh, the MPM effectively overcomes the mesh distortion issues common in large-deformation analyses (Soga *et al*. 2015, Qin *et al*. 2022). It has recently gained significant attention in geotechnical engineering, especially for simulating the behavior of multiphase soils. Various MPM formulations have been developed for both saturated and unsaturated conditions (Abe *et al*. 2013, Jassim *et al*. 2013, Martinelli 2016, Yerro *et al*. 2022, Kularathna *et al*. 2022). Liang *et al*. (2020) successfully demonstrated the effectiveness of a two-point MPM in modeling overtopping-induced dam failure. Other studies have also employed two-phase MPMs to capture the behavior of earth dams under different

*Corresponding author, Ph.D. Professor
E-mail: yhbyun@knu.ac.kr
[a]Graduate Student
[b]Postdoctoral Researcher
[c]Associate Professor

ISSN: 1229-9367 (Print), 1598-6233 (Online)

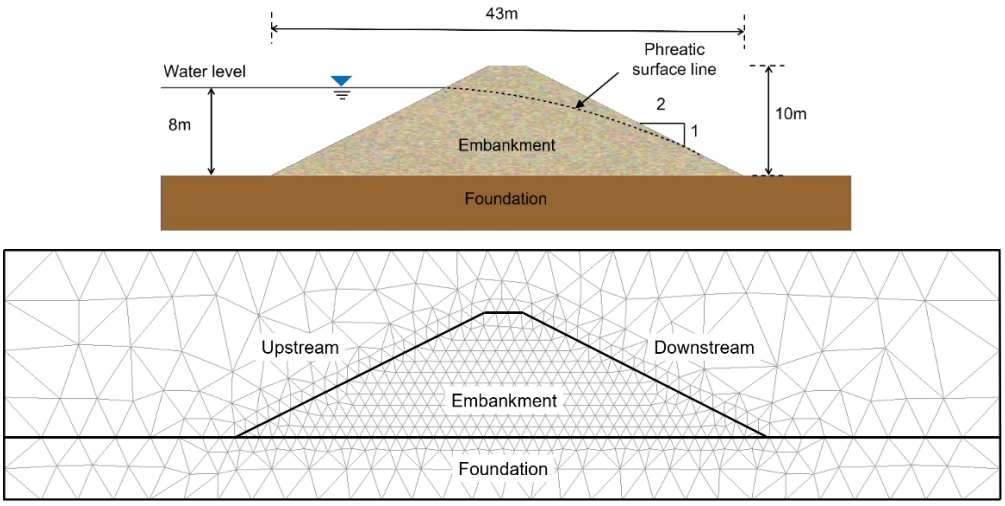

Fig. 1 Earth dam model and boundary conditions

hydraulic conditions (Ceccato *et al*. 2021, Girardi *et al*. 2021, Girardi *et al*. 2023a). Most recently, Kim *et al*. (2024) highlighted the effects of dam geometry, water level, and rainfall intensity on the behavior of earth dams. However, the MPM has yet to be employed to analyze earth dam behavior in relation to soil strength parameters or the relationship between slope stability and displacement.

This study explores the effect of soil strength parameters on the displacement behavior of earth dam models using a two-phase MPM. Across the following sections, the numerical framework and modeling approach are first introduced, including a brief description of the MPM and details of the simulation setup. The results of the numerical analyses, including failure evolution and displacement characteristics, are then presented. Finally, the effects of cohesion and internal friction angle on the displacement and FS are discussed.

2. Numerical study

2.1 Material point method

The computational procedure of the MPM comprises several sequential steps. First, all relevant state variables including kinematic and stress-related quantities are associated with the corresponding material points. These quantities are then projected onto the background mesh nodes using shape functions. The momentum balance equations are subsequently solved at the nodes, which yields the nodal accelerations. These nodal accelerations are then interpolated back to the material points to update their respective kinematic quantities. Thereafter, the strains and stresses at the material points are recomputed using a constitutive model. Finally, the material points are moved to their new positions, and the background mesh is restored to its original configuration. This mesh-resetting step prevents distortion during large deformations, thereby enhancing the numerical stability and accuracy of the simulation.

This computational strategy is implemented in the Anura3D code, which supports a two-phase single-point formulation. In the two-phase approach, saturated soils are modeled using a unified set of material points, with pore water pressure incorporated as an additional variable to represent coupled solid–fluid interactions (Conte *et al*. 2020). More details on the MPM are available in a previous publication (Kim *et al*. 2024b).

2.2 Simulation

Based on statistical data of earth dams in South Korea (RRI, 2011), a representative dam geometry was selected for modelling. The dam height was set to 10 m, representing the median value of the most commonly observed height range. The crest width was set to 3 m, and the upstream and downstream slopes were both assigned a horizontal-to-vertical ratio of 2:1. The water level on the upstream side was maintained at 8 m, which represents the full reservoir level in compliance with the freeboard criteria of the U.S. Army Corps of Engineers (2004). Regarding the initial condition, the phreatic line models obtained from a steady-state FEM seepage analysis was adopted to assign the initial pore water pressure distribution to the material points, as illustrated in Fig. 1. The material properties used for the dam models are summarized in Table 1. To ensure that failure would occur in the embankment rather than the foundation, the foundation soil was assigned a higher solid density and strength parameters than the embankment fill. Sand and clay embankments were assigned different hydraulic conductivities. A total 20 dam models were analyzed by varying the internal friction angle and cohesion of the embankment material. The values of the cohesion and friction angle for each dam model are listed in Table 2. All shear strength parameters used in this study fall within the typical ranges for sands and clays reported by South Carolina Department of Transportation (2022).

The domain in the MPM is defined as 80 m in width and 20 m in height. Triangular mesh elements are used, with mesh sizes set to 1 m for the embankment, 3 m for the foundation ground, and 5 m for the remaining regions. Based on this configuration, a total of 2,270 material points is generated. In contrast, the FEM mesh consists of square

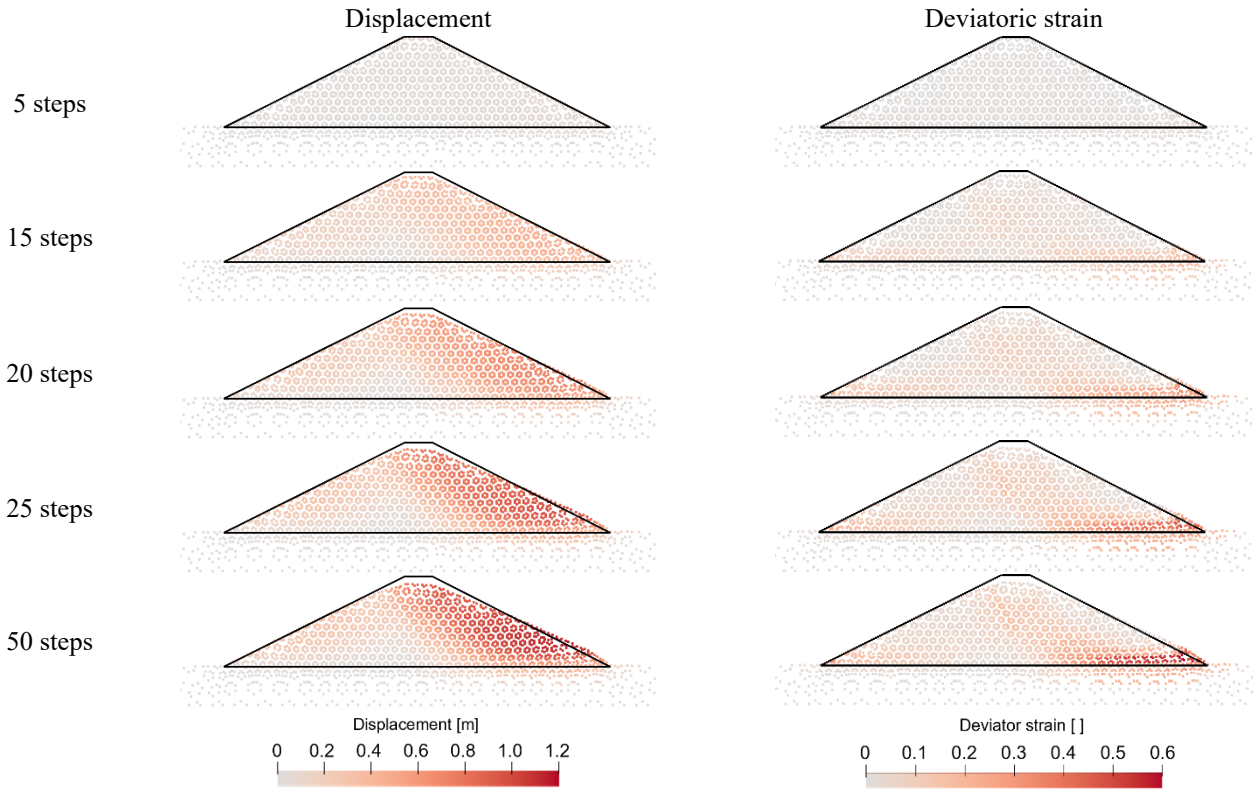

Fig. 2 Distributions and evolutions of displacement and deviatoric strain over time

Table 1 Material parameters for dam models

Material parameter	Value
Solid density [kg/m^3]	2100* / 2650†
Liquid density [kg/m^3]	1,000
Porosity [-]	0.3
Liquid bulk modulus [kPa]	80,000
Liquid dynamic viscosity [kPa·s]	$1 \cdot 10^{-6}$
Intrinsic permeability [m^2]	$1 \cdot 10^{-10}$ ‡ / $1 \cdot 10^{-12}$ §
Young's modulus [kPa]	30,000
Poisson ratio [-]	0.3

*solid density for embankment; †solid density for foundation; ‡permeability for sand; §permeability for clay

Table 2 Summary of strength parameters of dam models

Model	Friction angle [°]	Cohesion [kPa]	Model	Friction angle [°]	Cohesion [kPa]
S1	24	1	C1	15	10
S2	28		C2		15
S3	32		C3		20
S4	36		C4		25
S5	24	5	C5		40
S6	28		C6		55
S7	32		C7		70
S8	36		C8		100
S9	24	10			
S10	28				
S11	32				
S12	36				

elements with a uniform size of 1 m applied to both the embankment and the foundation ground. Note that a mesh size of 1 m for both FEM and MPM simulations was also adopted in previous studies (Sordo *et al*. 2022, Kim *et al*. 2024b). For the boundary conditions, the material points for both soil and water at the bottom of the domain are fixed in the horizontal and vertical directions. On both the left and right sides of the domain, the material points for soil are fixed in the horizontal direction only. While the computational time for the FEM analysis is approximately a few seconds per simulation, each case in the MPM model requires several hours to complete 10,000 steps, depending on the computing environment.

As a preliminary study, Kim *et al*. (2024b) used the same modeling approach to an earth dam and validated the MPM results by comparing them with FEM results. The spatial distribution of pore water pressure showed good agreement between MPM and FEM. More details on model validation can be found in Kim *et al*. (2024b).

3. Results and discussion

3.1 Failure evolution

To investigate the failure evolution, the distributions of the displacement and deviatoric strain within the embankment were examined. Fig. 2 presents the failure progression of a sand-filled dam model with a cohesion of

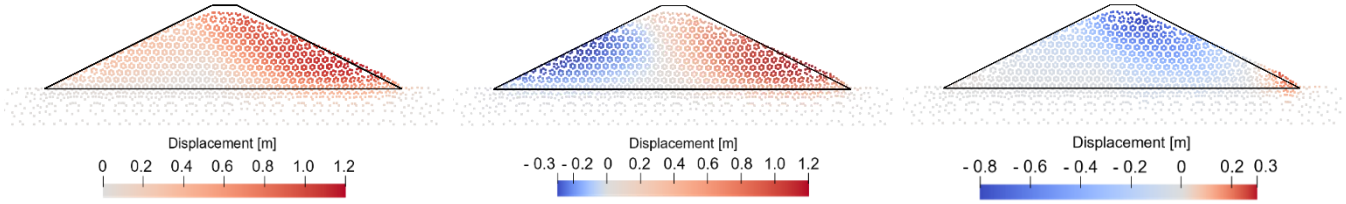

(a) Resultant direction (b) Horizontal direction (c) Vertical direction

Fig. 3 Displacement distribution at failure for internal friction angle of 24°

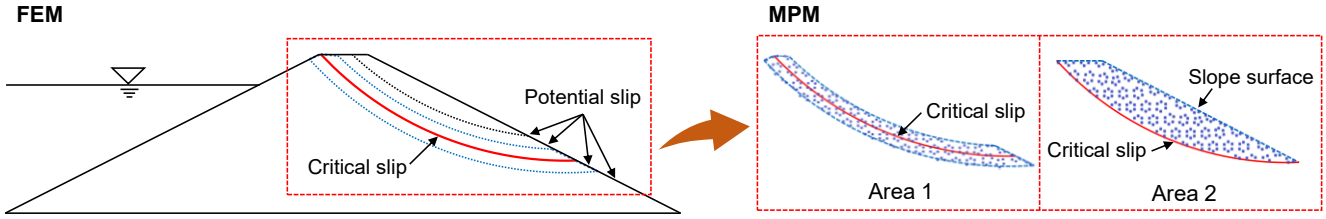

(a) Critical slip surface identified by FEM and corresponding zones for calculating average displacement

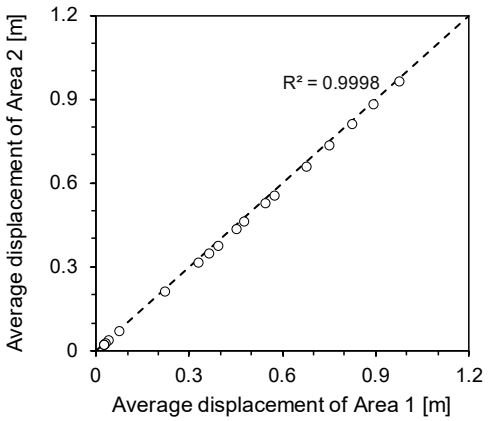

(b) Comparison of average displacements in Areas 1 and 2 obtained from MPM results

Fig. 4 Definition and comparison of average displacement regions in the embankment model

1 kPa and an internal friction angle of 24°. As the simulation progressed, the displacements began to localize along a circular slip surface in the downstream portion of the embankment. The deviatoric strain distributions clearly revealed the formation of shear bands and progressive failure initiating from the downstream toe. At Step 5, the embankment exhibited an almost uniformly negligible displacement field. By Step 15, displacements exceeding 0.4 m had developed in the downstream section, delineating a circular failure plane, while the negative pore pressure zone had propagated downward from the initial phreatic line. At step 20, differential movement between the upper and lower portions of the downstream slope became evident, with the maximum displacement occurring at the toe. The negative pore pressure region continued to extend further downward. After 25 steps, the dam crest became noticeably settled, and displacements greater than 0.9 m were observed in the lower part of the downstream slope. At Step 50, the maximum displacement, exceeding 1.1 m, was recorded at the downstream toe. By this stage, the displacement field converged displaying no further changes.

3.2 Displacement distribution

Fig. 3 presents the converged displacement distributions for the dam model with a cohesion of 1 kPa and an internal friction angle of 24°. Regardless of the friction angle, the shape and location of the slip surface remained nearly identical across all cases. Note that the displacement beneath the dam was mostly confined to the interface between the dam and foundation. The maximum displacement was consistently observed near the toe of the downstream slope. On the upstream slope, the maximum displacement was 0.33 m, corresponding to approximately 29% of the maximum displacement on the downstream slope. This result indicates that the upstream slope experienced significantly less deformation than the downstream slope.

Positive displacement in the horizontal direction indicates movement toward the downstream side of the dam, while positive displacement in the vertical direction implies upward movement. In the horizontal direction, the downstream slope showed positive displacement, while the

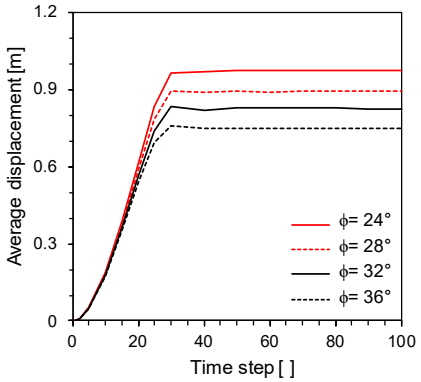

(a) 1 kPa

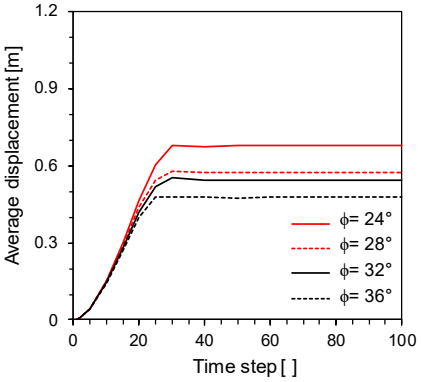

(b) 5 kPa

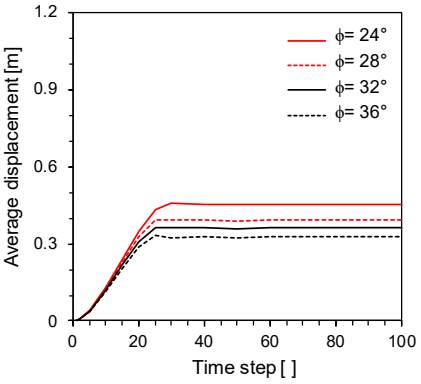

(c) 10 kPa

Fig. 5 Evolution of average displacement in sand-filled dam models under three different cohesions

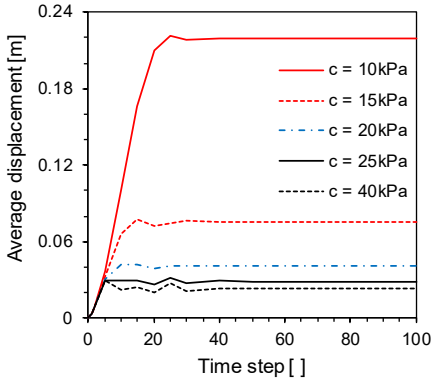

Fig. 6 Evolution of average displacement in clay-filled dam models under various cohesion

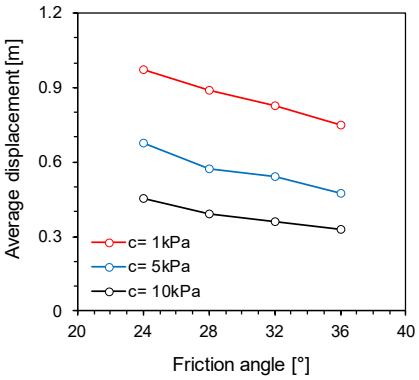

(a) Internal friction angle

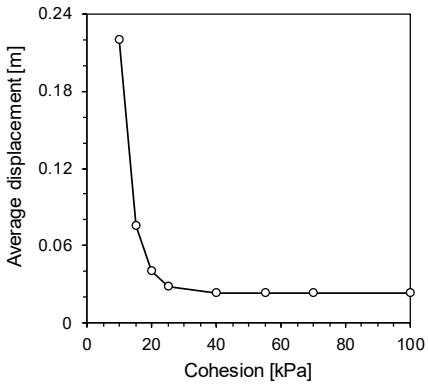

(b) Cohesion

Fig. 7 Variation in average displacements with strength parameters

upstream slope showed negative displacement. For a friction angle of 24°, the maximum horizontal displacement was approximately 1.14 m on the downstream side and −0.33 m on the upstream side. In the vertical direction, the maximum negative displacement consistently occurred at the dam crest, while the maximum positive displacement was observed near the downstream toe. For a friction angle of 24°, the crest displacement was approximately −0.83 m and the toe displacement reached +0.24 m.

3.3 Average displacement

The average displacement within a defined region of the dam model was calculated to represent the deformation associated with the failure surface independently of the overall embankment movement. As shown in Fig. 4(a), a slope stability analysis was first conducted using the FEM to identify the critical circular slip surface—defined as the surface with the lowest FS—on the downstream side of the embankment. Based on this slip surface, two zones were defined to compute the average displacement: Area 1, which extended 0.5 m on either side of the slip surface, and Area 2, which included the entire region above the slip surface. The average displacement in each zone was

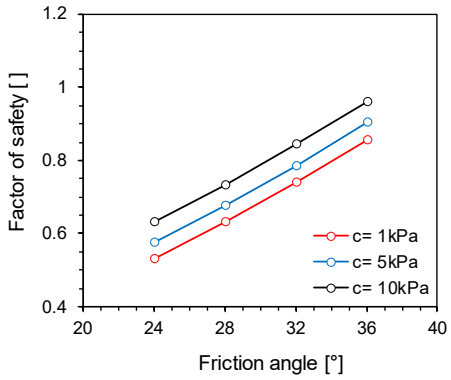

Fig. 8 Relationship between internal friction angle and factor of safety for sand-filled dam models

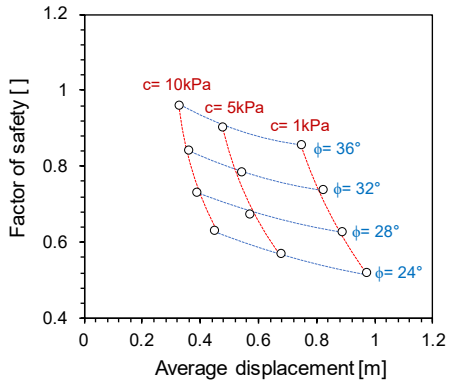

Fig. 9 Relationship among average displacement, factor of safety, and strength parameters in sand-filled dam models

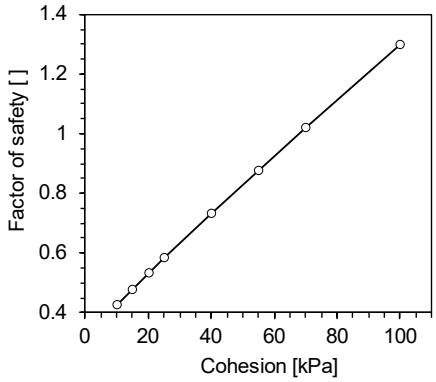

Fig. 10 Cohesion versus factor of safety

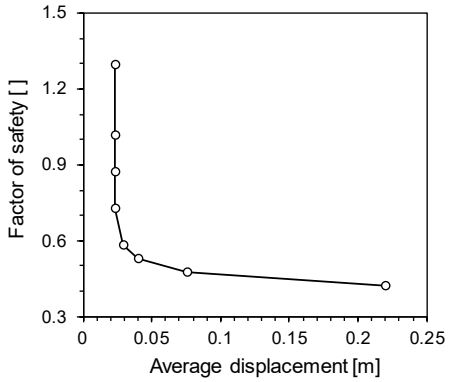

Fig. 11 Average displacement versus factor of safety

determined from the MPM simulation results. Fig. 4(b) compares the average displacements computed for Areas 1 and 2, highlighting an almost perfect correlation (R^2 = 0.9998) between the two measures across all models. This strong correlation suggests that either zone can provide a reliable representation of deformation behavior near the failure surface.

Fig. 5 shows the variation in average displacement in Area 2 during the early stages of the numerical analysis for the dam models constructed with sand. During the initial timesteps, the average displacement increased linearly, regardless of the strength parameter values. After approximately 20 timesteps, however, the displacement converged to different maximum values depending on the cohesion and friction angle. Lower cohesion values resulted in steeper slopes during the initial linear phase, which indicates that embankments with lower cohesion are more prone to rapid deformation. This trend is consistent with the findings of Harabinova and Panulinova (2022), who reported that increasing cohesion tends to reduce the rate at which the FS increases. Fig. 6 shows the variation in the average displacement during the initial timesteps for the clay-filled dam models with a constant internal friction angle. Overall, as observed with the sand-filled dam models, the average displacement increased linearly in the early stages before subsequently stabilizing. The maximum displacement occurred at later timesteps as the cohesion decreased. For cohesion values of 25 kPa or higher, the displacement exhibited a temporary instability before eventually converging. As the cohesion increased, the final converged displacement decreased, with nearly identical results observed for cohesion values of 40, 70, and 100 kPa.

3.4 Displacement versus strength parameters

The relationships between the converged average displacement of the embankment and the soil strength parameters are presented in Fig. 7. Fig. 7(a) shows the variation in the average displacement with the internal friction angle for sand-filled dam models with different cohesion values. At a given cohesion level, increasing the friction angle resulted in a nearly linear reduction in the average displacement. For instance, increasing the friction angle from 24° to 36° reduced the average displacement by approximately 0.225 m at a cohesion of 1 kPa, and by about 0.125 m at a cohesion of 10 kPa. This trend indicates that the influence of friction angle on displacement becomes less pronounced as cohesion increases. At a given friction angle, the average displacement clearly decreased with increasing cohesion. Specifically, increasing the cohesion from 1 kPa to 10 kPa reduced the displacement by about 0.520 m at a friction angle of 24°, and by approximately 0.421 m at a friction angle of 36°; the magnitude of the reduction was cohesion affects the displacement more significantly when

the friction angle is low. For the clay-filled dam models, Fig. 7(b) illustrates the variation in the average displacement with the cohesion. The average displacement decreased rapidly as the cohesion increased from 10 kPa to 25 kPa, while it remained nearly constant beyond approximately 25 kPa. These results suggest that a lower cohesion leads to larger displacements and that the sensitivity of the displacement to cohesion is higher within the low-cohesion range.

3.5 Displacement versus factor of safety

The FS of the downstream slope, obtained through a FEM analysis, was compared with the average displacement derived from the MPM results. Fig. 8 shows that for the sand-filled dam models, the FS of the downstream slope increased approximately linearly with the friction angle at a given cohesion value. Moreover, at a given friction angle, the FS increased with cohesion. Fig. 9 shows the relationship between the FS, the average displacement within the failure region, and the strength parameters. As the friction angle increased, the FS increased, whereas the average displacement decreased. Even at a fixed friction angle, increasing cohesion led to a higher FS and a lower average displacement. Overall, the FS and average displacement exhibited greater sensitivity to the friction angle and cohesion when both these strength parameters had low values. For the clay-filled dam models, the FS of the downstream slope increased almost linearly with cohesion, as shown in Fig. 10. However, Fig. 11 shows that unlike with the sand-filled models, the clay-filled models exhibited a reduction in FS—from approximately 1.30 to 0.58—with decreasing cohesion, which resulted in minimal change in the average displacement; this is consistent with the FS–displacement relationship reported by Hong *et al*. (2014). These results indicate that clay embankments with FS values near unity exhibit limited deformation, which hinders displacement-based stability assessment. Nevertheless, the relationship between FS and average displacement is useful not only for determining slope failure based on FS from FEM analysis but also for evaluating the post-failure behavior of earth dams.

4. Conclusions

In this study, a two-phase MPM was employed to simulate the failure behavior of earth dams under systematically varied shear strength parameters, namely cohesion and internal friction angle. The displacement characteristics and FS were analyzed for 20 numerical models using a combined MPM–FEM simulation approach. The key findings were as follows:

• The two-phase MPM modeling approach accurately captured the large-deformation mechanisms associated with embankment failure.

• In the sand-filled dam models, both cohesion and internal friction angle significantly influenced the average displacement and FS. The displacement decreased nearly linearly as the values of the strength parameters increased, exhibiting higher sensitivity to these parameters at lower values.

• The clay-filled dam models exhibited limited displacement under marginal FS conditions. This indicates that displacement-based stability assessments may not be suitable for highly cohesive embankments.

• The strong correlation between the MPM-derived displacements and the FEM-derived FS values demonstrated the applicability of this combined approach not only for identifying slope failure based on FS but also for evaluating the post-failure behavior of earth dams.

This study considered a limited number of dam models under idealized conditions. Future work incorporating various loading scenarios and rainfall events would further enhance the understanding of post-failure behavior in earth dams, which cannot be fully assessed through FS values alone.

Acknowledgments

This work was supported by a National Research Foundation of Korea (NRF) grant funded by the Korea government (MSIT) (No. NRF-2021R1A5A1032433).

References

Abe, K., Soga, K. and Bandara, S. (2013), "Material point method for coupled hydromechanical problems", *J. Geotech. Geoenviron. Eng.*, **140**(3), 04013033. https://doi.org/10.1061/(ASCE)GT.1943-5606.0001011.

Al-Janabi, A.M.S., Dibs, H., Sammen, S.S., Yusuf, B., Ikram, R.M.A., Alzuhairy, S.H. and Kisi, O. (2024), "Comparison analysis of seepage through homogenous embankment dams using physical, mathematical and numerical models", *Arab. J. Sci. Eng.*, 1-10. https://doi.org/10.1007/s13369-024-09224-x.

Anura3D (2024), ANURA3D version 2024 source code; Anura3D MPM Research Community. https://github.com/Anura3D/Anura3D_OpenSource.

Bui, H.H., Fukagawa, R., Sako, K. and Ohno, S. (2008), "Lagrangian meshfree particles method (SPH) for large deformation and failure flows of geomaterial using elastic-plastic soil constitutive model", *Int. J. Numer. Anal. Meth. Geomech.*, **32**(12), 1537-1570. https://doi.org/10.1002/nag.688.

Capecelatro, J. and Desjardins, O. (2013), "An Euler–Lagrange strategy for simulating particle-laden flows", *J. Comput. Phys.*, **238**, 1-31. https://doi.org/10.1016/j.jcp.2012.11.015.

Ceccato, F., Yerro, A., Girardi, V. and Simonini, P. (2021), "Two-phase dynamic MPM formulation for unsaturated soil", *Comput. Geotech.*, **129**, 103876. https://doi.org/10.1016/j.compgeo.2020.103876.

Choo, Y.W., Kim, Y.-H., Lee, J.H. and Kim, D.-S. (2014), "Reliability analysis of suction caissons for moored structures", *Geomech. Eng.*, **6**(1), 17-31. https://dx.doi.org/10.12989/gae.2014.6.1.017.

Girardi, V., Ceccato, F., Rohe, A., Simonini, P. and Gabrieli, F. (2023), "Failure of levees induced by toe uplift: Investigation of post-failure behavior using material point method", *J. Rock Mech. Geotech. Eng.*, **15**(4), 970-983. https://doi.org/10.1016/j.jrmge.2022.07.015.

Girardi, V., Yerro, A., Ceccato, F. and Simonini, P. (2021), "Modelling deformations in water retention structures with unsaturated material point method", *Proceedings of the Institution of Civil Engineers - Geotechnical Engineering*, **174**(5), 577-592. https://doi.org/10.1680/jgeen.21.00059.

Harabinova, S. and Panulinova, E. (2022), "Numerical analysis of slope stability", *IOP Conference Series: Materials Science and Engineering*, **1252**(1), 012084. https://doi.org/10.1088/1757-899X/1252/1/012084.

Jassim, I., Stolle, D. and Vermeer, P. (2013) salmasi, "Two-phase dynamic analysis by material point method", *Int. J. Numer. Anal. Meth. Geomech.*, **37**(15), 2502-2522. https://doi.org/10.1002/nag.2146.

Kim, D.J., Aregbesola, S.O., Lee, J.S., Cho, H. and Byun, Y.H. (2024a), "Image-based characterization of internal erosion around pipe in earth dam", *Comput. Concrete*, **33**(5), 481. https://doi.org/10.12989/cac.2024.33.5.481.

Kim, D.J., Lee, J.S., Bae, J.H., Son, D.G., Byun, Y.H. and Heo, Y.G. (2023), "Displacement field measurement of stacked geotextile tubes by digital image correlation", *Smart Geotech. Smart Soc.,* 813-816.

Kim, D.J., Park, G., Lee, J.S., Kang, T.H. and Byun, Y.H. (2024b), "Parametric study of earth dam failure simulation using material point method", *Steel Compos. Struct.*, **53**(6), 703-715. https://doi.org/10.12989/scs.2024.53.6.703.

Kodicherla, S.P.K. (2023), "Discrete element modelling of granular materials incorporating realistic particle shapes", *Int. J. Geo-Eng.*, **14**(1), 15.

Korea Rural Community Corporation Rural Research Institute (2011), "A study on development of the safety management & the data base for reservoir disaster prevention", Ansan, Korea.

Kularathna, S., Liang, W.J., Zhao, T.C., Chandra, B., Zhao, J.D. and Soga, K. (2022), "A semi implicit material point method based on fractional-step method for saturated soil", *Int. J. Numer. Anal. Meth. Geomech.*, **45**(10), 1405-1436. https://doi.org/10.1002/nag.3204.

Kumar, K., Soga, K. and Delenne, J.-Y. (2012), "Mechanics of granular column collapse in fluid at varying slope angles", arXiv:1211.4678 [physics.geo-ph]. https://arxiv.org/abs/1211.4678.

Liang, D., Zhao, X. and Soga, K. (2020), "Simulation of overtopping and seepage induced dike failure using two-point MPM", *Soils Foundations*, **60**(4), 978-988. https://doi.org/10.1016/j.sandf.2020.06.004.

Martinelli, M. (2016), "Soil-water interaction with material point method: Double-point formulation", Research Report No. MPM-Dredge PIAP-GA-2012-324522; EU-FP7 Research Project.

MIDAS Information Technology Co., Ltd., 2022. SoilWorks – computer software, v. 5.5.0.0.

Mkilima, T. (2022), "Modeling the impact of soil cohesiveness on embankment stability under rapid drawdown", *Technobius*, **2**(2), 0084. https://doi.org/10.54355/tbus/2.2.2022.0084.

Qin, J., Mei, G. and Xu, N. (2022), "Meshfree methods in geohazards prevention: A survey", *Archives Comput. Meth. Eng.*, **29**(5), 3151-3182. https://doi.org/10.1007/s11831-021-09686-4.

Rajabian, A. (2023), "Effect of initial failure geometry on the progress of a retrogressive seepage-induced landslide", *Int. J. Geo-Eng.*, **14**(1), 11. https://doi.org/10.1186/s40703-023-00189-8.

Salmasi, F., Norouzi, R., Abraham, J., Nourani, B. and Samadi, S. (2020), "Effect of inclined clay core on embankment dam seepage and stability through LEM and FEM", *Geotech. Geologic. Eng.*, **38**(6), 6571-6586. https://doi.org/10.1007/s10706-020-01455-7.

Soga, K., Alonso, E., Yerro, A., Kumar, K., and Bandara, S. (2016), "Trends in large-deformation analysis of landslide mass movements with particular emphasis on the material point method", *Géotechnique*, **66**(3), 248-273. https://doi.org/10.1680/jgeot.15.LM.005.

Sordo, B., Rathje, E. and Kumar, K. (2022), "Hybrid Finite Element and Material Point Method to Simulate Granular Column Collapse from Failure Initiation to Runout", *arXiv preprint*, arXiv:2206.07169. https://doi.org/10.48550/arXiv.2206.07169

South Carolina Department of Transportation (2022), Geotechnical Design Manual – Chapter 7: Geomechanics, South Carolina Department of Transportation; Columbia, SC, USA. https://dc.statelibrary.sc.gov/handle/10827/44854.

Sulsky, D., Chen, Z. and Schreyer, H.L. (1994), "A particle method for history-dependent materials", *Comput. Meth. Appl. Mech. Eng.*, **118**(1-2), 179-196. https://doi.org/10.1016/0045-7825(94)90112-0.

U.S. Army Corps of Engineers (2004), *General Design and Construction Considerations for Earth and Rock-fill Dams*, EM 1110-2-2300, U.S. Army Corps of Engineers; Washington, DC, USA. https://www.publications.usace.army.mil/Portals/76/Publications/EngineerManuals/EM_1110-2-2300.pdf.

Van Beek, V.M., De Bruijn, H.T.J., Knoeff, J.G., Bezuijen, A. and Förster, U. (2010), "Levee failure due to piping: A full-scale experiment", *Scour Erosion*, 283-292. https://doi.org/10.1061/41147(392)27.

Yerro, A., Girardi, V., Martinelli, M. and Ceccato, F. (2022), "Modelling unsaturated soils with the material point method: A discussion of the state-of-the-art", *Geomech. Energy Environ.*, **32**, 100343. https://doi.org/10.1016/j.gete.2022.100343.